JOURNAL OF APPLIED ELECTROCHEMISTRY 22 (1992) 787–794

Electrodeposition and characterization of amorphous Fe–Cr–P–C alloys

J.-C. KANG, S. B. LALVANI*

Mechanical Engineering and Energy Processes, Southern Illinois University-Carbondale, Carbondale, IL 62901, USA

Received 13 March 1991; revised 26 September 1991

Electrodeposition of iron–chromium alloys was investigated in a divided and undivided cell. The influence of the current density on the composition of the alloy was determined. Energy dispersive spectroscopy and Auger electron spectroscopy were used to evaluate alloy composition. These alloys were determined to be amorphous by X-ray diffraction and transmission electron microscopy. The corrosion behaviour of the alloys was studied in 0.5 M HCl, and they were found to be more corrosion resistant than conventional chromium electrodeposits, with corrosion currents ranging between 40–60 $\mu A\,cm^{-2}$, compared to 1850 $\mu A\,cm^{-2}$ for conventional chromium. The alloy electrodeposition mechanism was studied by cyclic voltammetry.

1. Introduction

Metallic glasses are amorphous or non-crystalline, like oxide glasses, but at the same time, they are different from the latter in several aspects. They are primarily composed of metallic elements and the interatomic bonding between them is essentially metallic in character. They are generally opaque rather than transparent, and they are not brittle; but their physical, chemical, and mechanical properties are similar to those of traditional materials, and generally superior to those of their crystalline counterparts.

Amorphous metals and alloys can now be produced by several techniques besides the rapid solidification of the metallic melts, a commonly used method. The better known methods for amorphous alloy production are the conventional wet electrodeposition process and other dry processes such as ion sputtering [1–3], ion implantation [4, 5], and laser glazing [6].

Electrodeposition of amorphous Fe–Cr–P alloys has been carried out by Ng *et al.* [7, 8]. The alloys were deposited from an acidic citrate electrolyte using sodium hypophosphite as the source of phosphorous. A Nafion®† cation selective membrane separating the anode from the cathode was used to avoid possible interference from the oxidation of Cr^{3+} to Cr^{6+} at the anode. They found a maximum current efficiency of 20% at a current density of 100 $mA\,cm^{-2}$ which resulted in the formation of an alloy containing 10 at % Cr at 19 at % P. At higher current densities (200–300 $mA\,cm^{-2}$), the current efficiency dropped to less than 10% and the deposits appeared rough with unplated pin holes.

In this paper, we report a method for Fe–Cr–P–C electrodeposition. Hashimoto *et al.* [9–12] have studied the passive film on Fe–Cr alloys prepared by centrifugal quenching from a liquid melt. They found that the passive film consists mainly of hydrated chromium oxyhydroxide which is a major constituent of passive films on crystalline stainless steels. In this work carbon, a metalloid, is added (as an organic agent) to the deposit to facilitate the amorphous phase formation. Addition of phosphorous and carbon also leads to improvement in the corrosion resistance of metallic glasses containing iron and chromium [13]. It must be stated at the outset that although the carbon inclusion is in the form of an organic agent in the deposit, for the sake of brevity deposits produced in this study are referred to as Fe–Cr–P–C.

2. Experimental procedure

2.1. *Electrodeposition*

The alloys were electrodeposited using the bath shown in Table 1. The electrolyte was prepared with distilled water and reagent grade chemicals. Sulphuric acid and sodium hydroxide were used for pH adjustments of the bath. In some experiments, a cation selective Nafion® membrane was used to separate the anode compartment from the cathode. The cathode was made of copper, either in the shape of a disc or foil. The copper discs, after roughening on a wet belt sander with 180 grit SiC paper, were polished with 240, 320, 480, and 600 grit wet SiC paper. Then the discs were polished with 6 μm diamond particles, followed by 1.0 μm and 0.05 μm Al_2O_3 powders. The substrates were degreased with acetone prior to deposition. The anode was a platinum mesh. Electrodeposition was carried out at room temperature galvanostatically at 20 to 90 $A\,dm^{-2}$.

The faradaic efficiencies were calculated using the compositional analysis obtained by energy dispersive

* Author to whom all correspondence should be addressed.
† Trade mark of the Du Pont Company.

0021-891X/92

Table 1. Bath composition for Fe–Cr–P–C deposition

$Cr_2(SO_4)_3 \cdot nH_2O$ (19.5% Cr)	167 g dm^{-3}
$Fe(NH_4)(SO_4)_2 \cdot 12H_2O$	40 g dm^{-3}
NaH_2PO_2	10 g dm^{-3}
$(NH_4)_2SO_4$	80 g dm^{-3}
K_2SO_4	20 g dm^{-3}
Sodium citrate	45 g dm^{-3}
Citric acid	30 g dm^{-3}
Boric acid	40 g dm^{-3}
Formic acid	50 cm^3 dm^{-3}

pH 1.0–2.0; temperature = 30° C

X-ray analysis (EDS). The equipment available for this analysis did not detect carbon, so efficiency calculations were based on Fe, Cr, and P compositions.

2.2. *Corrosion measurements*

Corrosion measurements were made by performing potentiodynamic polarization scans according to the American Society of Testing and Materials (ASTM) method G5-82. The corrosion measurements were obtained with an EG&G Princeton Applied Research Model 273 potentiostat/galvanostat and a Softcorr Corrosion Measurements Model 342 software was used to calculate corrosion potentials, corrosion currents and Tafel slopes [14]. Platinum mesh was used as the counter electrode; a saturated calomel electrode was used as the reference electrode and the electrodeposited alloy mounted in a Teflon holder was used as the working electrode. The specimen was immersed for 1 hour before initiating polarization. The corrosion potential (E_{corr}) against time was recorded and indicated that E_{corr} reached a steady-state before the scan was started. A potentiodynamic potential scan rate of 0.2 mV s^{-1} was used to record the current continuously with change in potential.

2.3. *Composition and structure*

The alloy composition was determined by energy dispersive X-ray analysis (EDS), and Auger electroscopy (AES). The surface was cleaned prior to analysis. The alloy was sputtered to a depth of 50 nm for AES. The structure of the alloys was determined by X-ray diffraction (XRD) and transmission electron microscopy (TEM). Diffraction was performed in a 2θ angle of 5° to 144°. A copper target was used with a diffracted beam monochromater. A Hitachi H-500H transmission electron microscope was used for TEM analysis. A 3 mm specimen was drilled from the deposited alloys and dimpled by a VCR Group Dimpler. The dimpled specimen was then milled at liquid nitrogen temperature. The cross-sectional surface of the electrodeposits polished with 0.05 μm Al_2O_3 and then etched with concentrated HCl was examined using scanning electron microscopy (SEM).

2.4. *Cyclic voltammetry*

The electrolyte was prepared in the same manner as the plating bath. Nitrogen was purged through the electrolyte approximately 10 min prior to testing. The programmable potentiostat used for performing cyclic voltammetry was the BioAnalytical System Model 100. A three-electrode cell containing a platinum wire for the counter electrode, a glassy carbon microelectrode (diameter 3.2 mm) for the working electrode, and a Ag/AgCl reference electrode were used.

3. Results and discussion

3.1. *Electrodeposition studies*

Iron–chromium–phosphorous–carbon alloys were deposited from the bath listed in Table 1. Potassium sulphate was included to enhance the bath conductivity. Ammonium sulphate is a complexant possibly in the high pH of the diffusion layer. Sodium citrate and citric acid served as bath complexing and buffering agents. Boric acid (pK $\cong$ 9) as a borate complex could possibly act as a buffering agent. The chief acid/base buffer in the bath is the aquochromium(III) ion (pK $\cong$ 4). Formic acid was also added since it is known to enhance the appearance of the deposits [15–17]. It also acted as a source of carbon.

A cation selective Nafion® membrane was used to separate the catholyte from the anolyte in some cases. Tables 2 and 3 show the composition of electrodeposits produced under identical conditions with and without Nafion® membrane, respectively, as determined by EDS. The presence of the membrane resulted in lowering of the chromium content of the deposits. In a previous report [7], investigators used a Nafion® membrane so that Cr^{6+}, an oxidation product at the anode, was prevented from undermining the deposit produced at the cathode. No such deleterious effect in the undivided cell was observed in our experiments for Fe–Cr–P–C deposition. However, when Cr–P–C deposits are produced, the separation of anode from the cathode is preferred [18, 19].

Thus, we presume that due to their high corrosion resistance, Fe–Cr–P–C deposits are not degraded by Cr^{6+}. It is possible that reduction of both Cr^{3+} and Cr^{6+} to Cr occurs at the cathode. Since Cr^{6+} is easier to deposit than Cr^{3+}, chromium content of the deposits in the undivided cell is found to be greater than that obtained using the cation selective membrane. It is also known that the rate of deposition is greater for Cr^{6+} than Cr^{3+} baths [20, 21].

The faradaic current efficiencies for deposition were found to be very low for experiments conducted in the divided cell, and the thickness of the deposits was only a few microns. Previous studies performed using divided cells [7, 8] with baths similar to the one used in this study have shown that the current efficiency decreases with current density (in the study cited formic acid was not added to the plating bath). Our data show the current efficiency increased with the current density and reached a maximum of $\sim$10% (Table 2). The chromium content of the deposits was also found to increase with the current density. Since,

*Table 2. Composition of Fe–Cr–P–C thin films as determined by EDS**

Expt. no.	*Current density/ A dm^{-2}*	*Composition/at %*			*Current efficiency/%*	*Thickness/ μm*
		Fe	*Cr*	*P*		
A	20	75	7	18	2	6
B	30	75	11	14	1	4
C	65	65	24	11	10	31
D	90	63	28	9	7	11

* The deposits were produced on a copper foil. A Nafion® cation membrane was used to separate the electrodes. A total charge of 900 C was passed. Deposition conditions as in Table 1.

chromium has the most negative standard electrode potential as compared to that of the other electroactive species present in the plating bath, its deposition rate is favoured at higher current densities. The Cr content of the deposits ranged from 7 to 28 at % (divided cell). Both the P, as well as Fe content of the deposits, decreased with the current density. The current efficiencies for alloy deposition are much higher (20–39%) when an undivided cell was used (Tables 2 and 3). The current efficiency appears to be a function of the substrate as well. For example, the current efficiency was estimated to be 82% greater for a deposit produced on a copper disc than the corresponding efficiency for deposition on a copper foil. A number of experiments were conducted to determine the reproducibility of the data reported in Table 3. Very good to satisfactory reproducible data were obtained for experiments conducted in the undivided cell.

3.2. *Deposit characterization*

The X-ray diffraction patterns for most of the Fe–Cr–P–C deposits showed only a broad peak around the 2θ angle of 43.35°. This broad peak suggests that the Fe–Cr–P–C deposits may be considered amorphous in structure. Figure 1 shows a typical XRD pattern of an amorphous $Fe_{38}Cr_{56}P_6C$ deposit. It is interesting to note that although the phosphorous content (as determined by EDS) of the deposit is very low, the deposit appears to be amorphous. We believe the structure is amorphous in part due to its relatively high carbon content (which could not be determined by the EDS unit available to us). Data regarding the carbon content of the deposits as discussed below. Transmission electron microscopy (TEM) was also performed on samples containing different compositions. The selected area diffraction patterns (SADPs) of $Fe_{75}Cr_{11}P_{14}C$ (Expt. B, Table 2) and $Fe_{38}Cr_{56}P_6C$ (Expt. E, Table 3) are shown in Figs 2 and 3, respectively. The SADPs of both 11 and 56 at % Cr deposits are essentially identical. They consisted of a prominent diffuse ring and some subsidiary fainter outer rings. The bright field images were found to be generally uniformly mottled, indicating an amorphous structure.

The Fe–Cr–P–C deposits were found to contain carbon and oxygen as determined by Auger electron spectroscopy (AES). The surface of the deposit was found to be covered with an oxide layer, as indicated in the AES depth profile (Fig. 4). This oxide layer is about 5–10 nm in thickness and is probably a mixture of iron oxides and chromium oxides. Table 4 shows a comparison of compositional analysis between AES and EDS techniques on a thin film produced at 30 A dm^{-2} (Expt. E, Table 3). The surface carbon content is very high (43 at %) presumably due to the environmental impurities, but in the bulk it corresponds to about 11 at %. Similarly, the oxygen content decreases upon sputtering and corresponds to about 14 at % in the bulk. Thus, the electrodeposit contains a total metalloid content of about 19 at % (8%P + 11%C).

Figure 5 is a SEM micrograph of an etched $Fe_{37}Cr_{55}P_8C$ deposit (Expt. F, Table 3). The deposit obtained on a copper disc was cut to half. The cross section of the deposit was etched by hydrochloric acid. Microcracks were observed on the surface of the deposit (Fig. 5a), which were formed during plating when the tensile stress exceeded the cohesive strength of the alloy. The cross section of the deposit shows layers formed during plating (Fig. 5b). It is interesting to note that the layers are more condensed near the substrate than near the surface. Figure 6 shows the surface and cross section of the deposit heat treated at

*Table 3. Composition of Fe–Cr–P–C thin films as determined by EDS**

Expt. no.	*Current density/ A dm^{-2}*	*Composition/at %*			*Current efficiency/%*	*Thickness/ μm*
		Fe	*Cr*	*P*		
E	30	38	56	6	21	34
F	30†	37/29	55/57	8/13	39/21	40/25
G	50	31	64	5	21	30

* Deposition was carried out in an undivided cell. The deposits were produced on a copper foil by passing a charge of 1000 C. Deposition conditions as in Table 1.
† Produced on a copper disc.

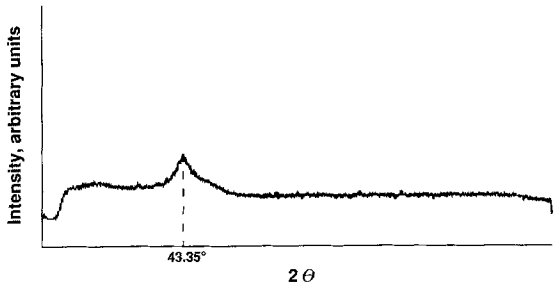

Fig. 1. The X-ray diffraction pattern of $Fe_{38}Cr_{56}P_6C$ deposit (Expt. E in Table 3).

300° C. More cracks were formed during the heat treatment. The cracks observed in as-plated and heat treated deposits are characteristic of electrodeposited chromium films.

3.3. *Corrosion measurements*

Potentiodynamic polarization curves of two amorphous deposits with different compositions are shown in Fig. 7. The alloy containing phosphorous and carbon were found to be less active based on the corrosion data provided in Table 5. This result is in agreement with the investigations of Naka *et al.* [13] who stated

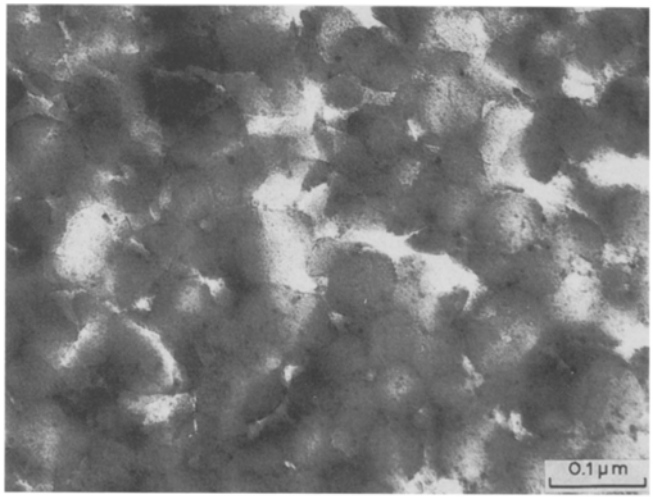

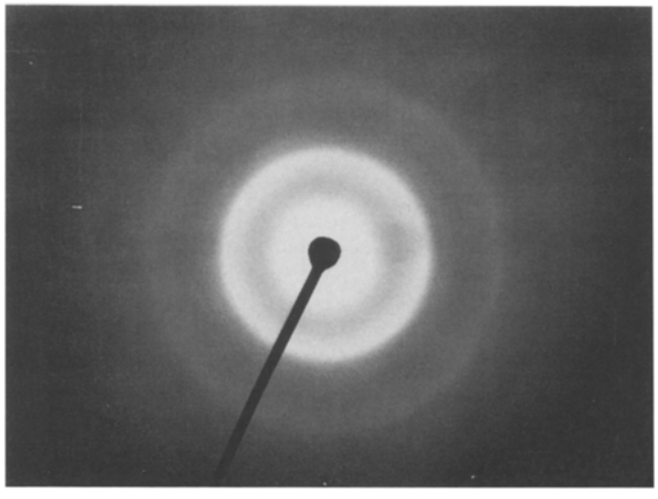

Fig. 2. TEM analysis of amorphous $Fe_{75}Cr_{11}P_{14}C$ deposit (Expt. B in Table 2).

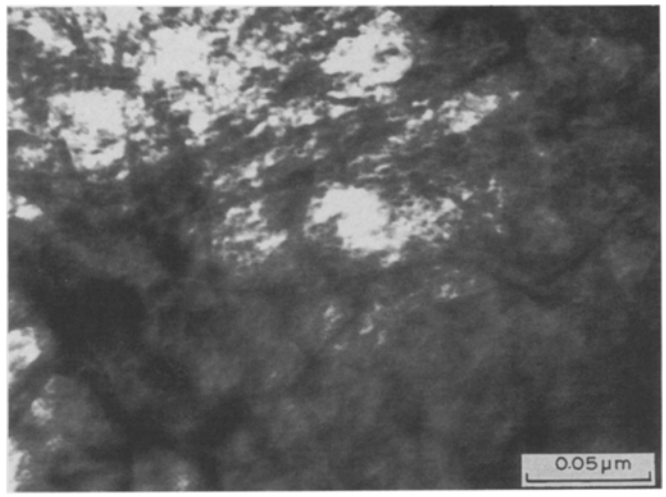

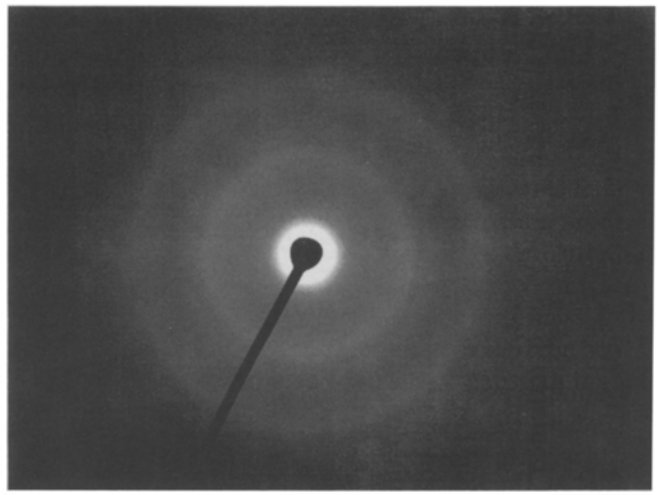

Fig. 3. TEM analysis of amorphous $Fe_{38}Cr_{56}P_6C$ deposit (Expt. E in Table 3).

that the combination of P and C results in an extremely high corrosion resistance in Fe–Cr-based amorphous alloys. The alloys are observed to passivate in the potential range of −0.3–0.0 V/SCE. It is interesting to observe that as compared to the amorphous alloys, Cr coating electrodeposited from Sargent's bath [20, 21] showed much higher corrosion currents. The high corrosion resistance of the alloys can result partly from the presence of chromium and large amounts of phosphorous and carbon, and partly from a homogeneous single phase amorphous structure. Sorensen *et al.* [22] have ascribed the excellent corrosion resistance of Fe–Cr–P alloys in chloride environment to the presence of phosphorous. According to them, P

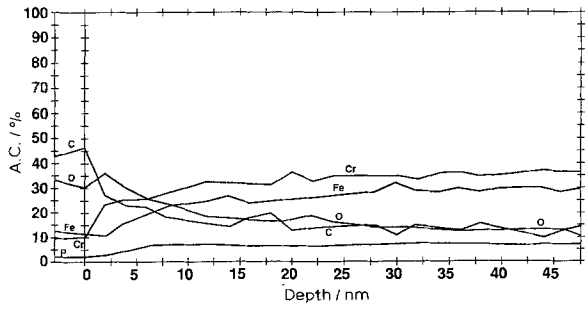

Fig. 4. Depth profile of composition determined by AES of $Fe_{38}Cr_{56}P_6C$ deposit (Expt. E in Table 3).

Table 4. A comparison of compositional analysis between AES and EDS on an Fe–Cr–P–C thin film (Expt. E in Table 3)

	AES/at %		*EDS/at %*
	Surface	*Under 500 A*	
Fe	15	30	38
Cr	10	37	56
P	3	8	6
C	43	11	–
O	34	14	–
FeO	–	–	37*
Cr_2O_3	–	–	57*
P_2O_5	–	–	6*

* Estimated values.

implantation to Fe–Cr alloys at low Cr concentration (6%) increases the rate of passivation and the quality of the passive film in sulphate solutions. However, chloride ions can break the passive films. If sufficiently high Cr concentration in the alloy is present, the alloy

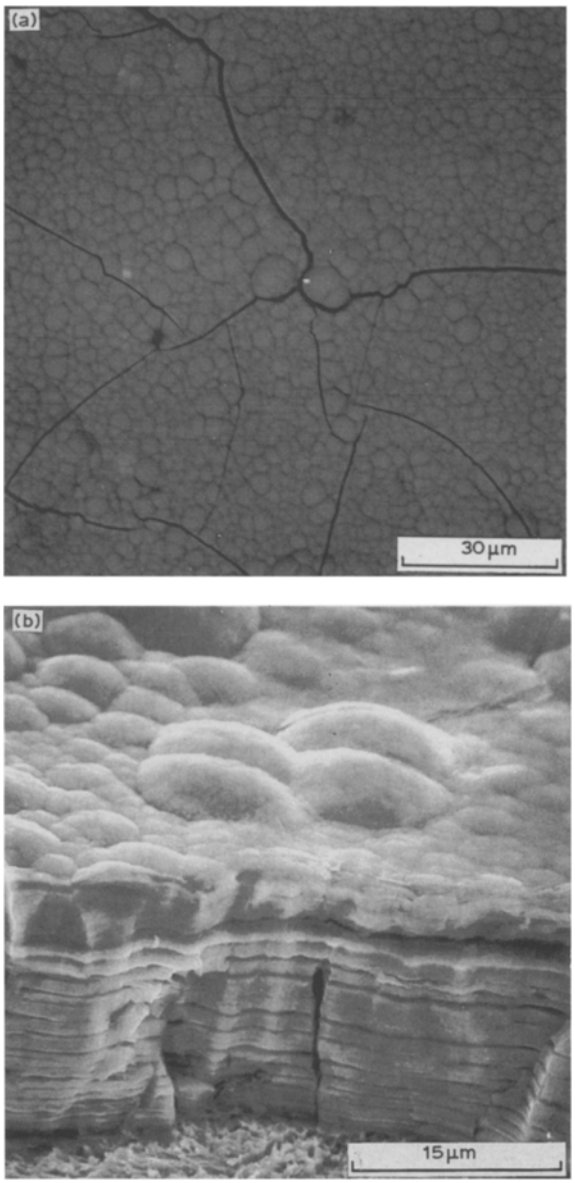

Fig. 5. SEM photomicrograph of a $Fe_{37}Cr_{55}P_8C$ deposit (after etching). (a) Surface and (b) cross section.

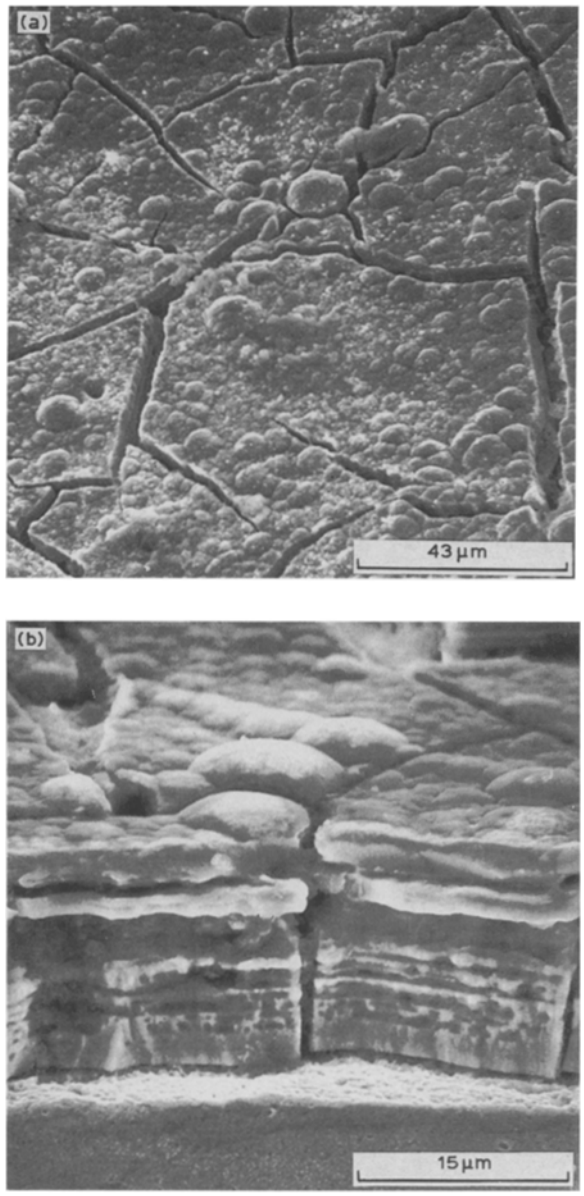

Fig. 6. SEM photomicrograph of a heat treated (450°C) $Fe_{37}Cr_{55}P_8C$ deposit (after etching. (a) Surface and (b) cross section.

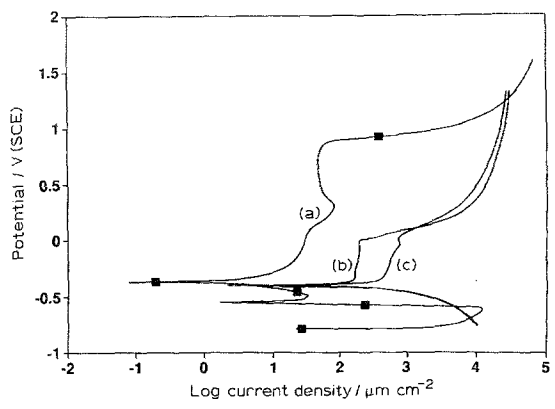

Fig. 7. Potentiodynamic polarization curves of Fe–Cr–P–C amorphous deposits in 0.5 M HCl. (a) Cr–X–, (b) $Fe_{66}Cr_{26}P_8C$ and (c) $Fe_{81}Cr_8P_{11}C$.

Table 5. A comparison of corrosion data for Fe–Cr–P–C alloys in 0.5 M HCl

Expt. no.	Alloys	E_{corr}/ mV (SCE)	I_{corr}/ $\mu A\,cm^{-2}$
1	$Fe_{81}Cr_8P_{11}C$	−404	63
2	$Fe_{66}Cr_{26}P_8C$	−392	37
3	Conventional chromium	−793	1850

is passivated in both chloride and sulphate solutions. Our data are supported by those of Sorensen *et al.* [22].

3.4. *Cyclic voltammetry*

Figure 8 shows a cyclic voltammogram which was obtained using the plating bath used for deposition except that no chromium, phosphorous and carbon-containing compounds were present. The peak for reduction of iron on glassy carbon electrode was observed on the forward scan (in the negative direction) at about −0.4 V against Ag/AgCl (Peak A). The standard electrode potential for Fe^{3+}/Fe^0 is −0.16 V against Ag/AgCl (also see Fig. 9, where the peak A appears larger since the forward scan is stopped before the iron nucleation potential). When scanning was continued to more negative potentials, a sharp peak (B) was observed at −1.4 V against Ag/AgCl which we ascribe to the nucleation of iron on iron deposited at −0.4 V against Ag/AgCl. On the reverse scan, an anodic peak was observed at −0.42 V against Ag/AgCl.

In order to show that peak B (Fig. 8) is due to iron nucleation, the following experiment was performed. Bulk electrodeposition on the glassy carbon electrode was performed at −1.0 V against Ag/AgCl, and a charge of 10 coulombs was passed. The electrode was then found to be totally covered with iron (visual observation). Cyclic voltammetry on the iron-deposited electrode was performed (Fig. 10), and a sharp peak was observed at −1.3 V against Ag/AgCl, which is about the same potential as in peak B (Fig. 8). No peak corresponding to the peak A of Fig. 8 was observed. Moreover, the peak current corresponding to peak B in Fig. 10 is more than five times in magnitude than the corresponding peak in Fig. 8. This

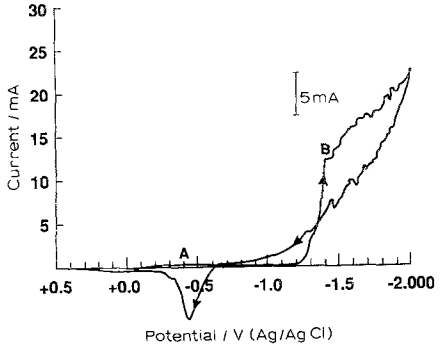

Fig. 8. Cyclic voltammogram of $Fe(NH_4)_2SO_4 \cdot 12H_2O$ on a glassy carbon electrode. Solution used is shown in Table 1 to which Cr source, formic acid, and NaH_2PO_2 were not added; scan rate = 100 mV s^{-1}; low E = −2.0 V against Ag/AgCl.

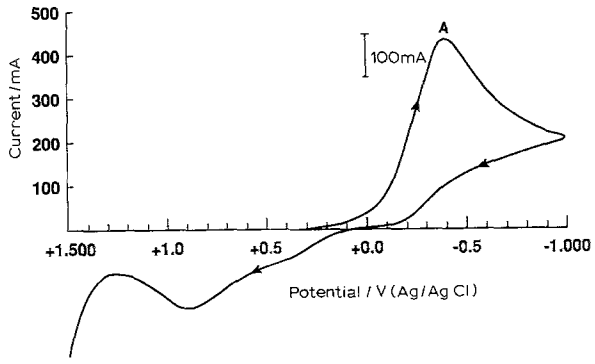

Fig. 9. Cyclic voltammogram of $Fe(NH_4)_2SO_4 \cdot 12H_2O$ on a glassy carbon electrode. Solution used as in Fig. 8; scan rate = 100 mV s^{-1}, low E = −1.0 V against Ag/AgCl.

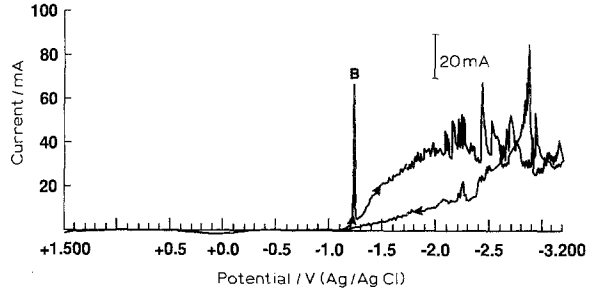

Fig. 10. Cyclic voltammogram of $Fe(NH_4)_2SO_4 \cdot 12H_2O$ on an iron-deposited glassy carbon electrode. Bulk deposition of iron was carried previously, using the solution indicated in Fig. 8; scan rate = 100 mV s^{-1}.

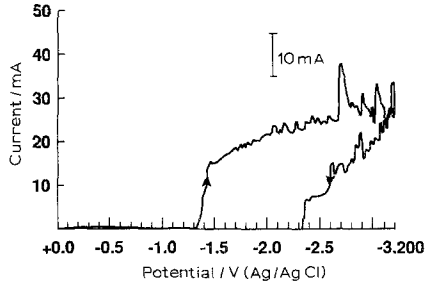

Fig. 11. Cyclic voltammogram of Fe–P system on a glassy carbon electrode. Solution used is shown in Table 1 to which Cr source and formic acid were not added; scan rate = 100 mV s^{-1}.

indicates that iron only partially covered the glassy carbon electrode on which bulk electrolysis was not performed.

Figure 11 is the cyclic voltammogram obtained on a glassy carbon electrode in a plating bath in which chromium and carbon sources were not added. It is interesting to observe that no anodic currents were observed (during reverse scan) in the potential range examined. This suggests that oxidation of the alloy is inhibited presumably due to phosphorous addition. The nucleation potential of Fe–P–C (Fig. 12) shifted to a slightly less negative potential of −1.2 V against Ag/AgCl as compared to Fe–P alloy. Again no oxidation peak was observed. The cyclic voltammograms for (i) Fe–Cr–P, and (ii) Fe–Cr–P–C systems are shown in Figs 13 and 14, respectively. A comparison of these two voltammograms clearly shows that the nucleation potential is shifted to more negative values

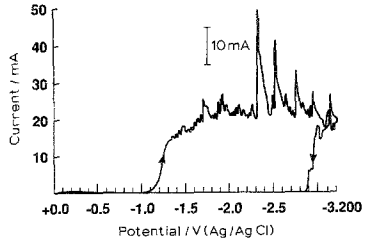

Fig. 12. Cyclic voltammogram of Fe–P–C system on a glassy carbon electrode. Solution used is shown in Table 1 to which Cr source was not added; scan rate = 100 mV s^{-1}.

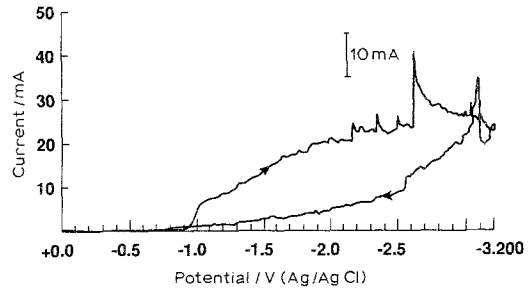

Fig. 13. Cyclic voltammogram of Fe–Cr–P system on a glassy carbon electrode. Solution used is shown in Table 1 to which formic acid was not added; scan rate = 100 mV s^{-1}.

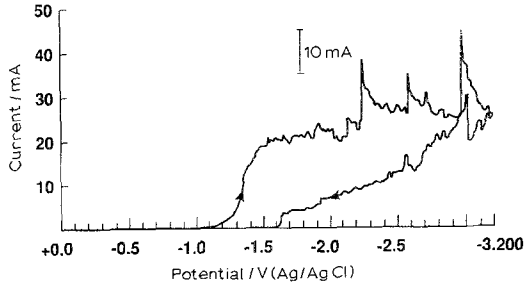

Fig. 14. Cyclic voltammogram of Fe–Cr–P–C system on a glassy carbon electrode. Solution used is shown in Table 1; scan rate = 100 mV s^{-1}.

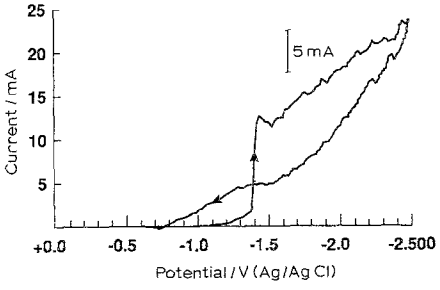

Fig. 15. Cyclic voltammogram of Cr^{3+} on a glassy carbon electrode. Solution used is shown in Table 1 to which Fe and P sources, and formic acid were not added; scan rate = 100 mV s^{-1}.

due to the formic acid (i.e., carbon source) addition. No anodic peaks were observed during the reverse scan.

Howarth and Pletcher [23] observed a nucleation potential of −1.34 V against Ag/AgCl for $Cr^{3+} \rightarrow Cr$. The standard electrode potential for Cr^{3+}/Cr^0 is −0.54 V against Ag/AgCl. Figure 15 is a cyclic voltammogram obtained in the plating bath which does not contain iron, phosphorous, and carbon source (i.e. it contains only Cr^{3+}). The nucleation peak for Cr^{3+}/Cr^0 is observed at −1.4 V against Ag/AgCl. It is

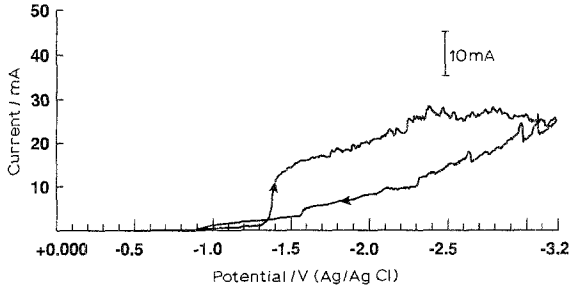

Fig. 16. Cyclic voltammogram of Cr–C system on a glassy carbon electrode. Solution used is shown in Table 1 to which Fe and P sources were not added; scan rate = 100 mV s^{-1}.

also noteworthy that a small anodic peak was observed at −0.72 V against Ag/AgCl. With the addition of formic acid (Fig. 16), the nucleation peak did not shift, however, the anodic peak disappeared completely. The data thus suggest that inclusion of carbon could inhibit the corrosion of chromium.

4. Conclusions

A new bath for electrodeposition of amorphous Fe–Cr–P–C thin films has been tested. Alloy deposition can be caried out from an undivided cell with relatively favourable faradaic current efficiencies. The corrosion behaviour of these alloys is very distinct from the conventional chromium. The amorphous alloys had corrosion currents on the order of 30 times less and corrosion potentials more noble than those of the conventional chromium in 0.5 M HCl. Microcracks were observed in the thin film produced. The cyclic voltammetry data show that the rate of iron deposition is greater on iron nucleation sites than on carbon. The inclusion of formic acid shifts the nucleation potentials to a more negative value.

Acknowledgements

Financial support from the Materials Technology Center, Southern Illinois University is gratefully acknowledged.

References

[1] L. D. McCormick, N. S. Wheeler and E. K. Williams, *J. Res. Natl. Bur. Stand.* **44** (1950) 109.
[2] R. Wang and M. D. Merz, *Corrosion* **40** (1984) 272.
[3] N. L. Lee and R. Schulz, *J. Mater. Res.* **3** (1988) 862.
[4] A. W. Grant, A. Ali, L. T. Chadderton, P. J. Grundy and E. Johnson, 'Rapidly Quenched Metals II' (edited by B. Cantor), 1 (1978) 63.
[5] V. Ashworth, D. Baxter, W. A. Grant and R. P. M. Proctor, *Corros. Sci.* **16** (1976) 775.
[6] T. R. Anthony and H. E. Cline, *J. Appl. Phys.* **49** (1978) 1248.
[7] P. K. Ng, T. E. Mitchell, I. E. Locci and A. A. Ruiz, *J. Mater. Res.* **4** (1989) 300.
[8] P. K. Ng and R. F. Paluch, 'Electrodeposition of Iron–Chromium–Phosphorous Amorphous Alloys', Extended Abtracts 85-2. The Electrochemical Society Meeting at Las Vegas, NV, October 13–18 (1985) p. 328.
[9] K. Asami, K. Hashimoto and S. Shimodaira, *Corr. Sci.* **16** (1976) 35.
[10] K. Hashimoto, K. Osada, T. Masumoto and S. Shimodaira, *ibid.* **16** (1976) 71.
[11] K. Asami, K. Hashimoto and S. Shimodaira, *ibid.* **16** (1976) 387.

[12] *Idem, ibid.* **16** (1976) 909.
[13] M. Naka, K. Hashimoto and T. Masumoto, *J. Non-Cryst. Solids* **28** (1978) 403.
[14] "Softcorr" Corrosion Measurement Software Model 342 Version 2.38, Princeton Applied Research Corporation, Electrochemical Instruments Division, CN5206, Princeton, NJ 08543 (1986).
[15] A. M. Kasaaian and J. Dash, *Plat. & Surf. Finish.* **71** (1984) 66.
[16] S. Hoshino, H. A. Laitinen and G. B. Hoflund, *J. Electrochem. Soc.* **133** (1986) 681.
[17] I. Drela, J. Szynkarczuk and J. Kubicki, *J. Appl. Electrochem.* **19** (1989) 933.
[18] V. V. Bondar and I. I. Potapov, *Zashchita Metallov* **5** (3) (1969) 346–8.
[19] B. A. DeNeve and S. B. Lalvani, 'Electrodeposition and Characterization of Amorphous Cr–P–C Alloys', submitted to *J. Appl. Electrochem.*
[20] F. A. Lowerheim, Editor, 'Modern Electroplating', 3rd edition, John Wiley and Sons, New York (1974).
[21] A. Brenner, 'Electrodeposition of Alloys', Vol. I, Academic Press, New York (1963).
[22] N. R. Sorensen, R. B. Diegle and S. T. Picraux, *Corrosion* **43** (1987) 2.
[23] J. N. Howarth and D. J. Pletcher, *J. Appl. Electrochem.* **18** (1988) 644.